Journal of Computational Physics 255 (2013) 1–15

Contents lists available at ScienceDirect

Journal of Computational Physics

www.elsevier.com/locate/jcp

Generalized multiscale finite element method. Symmetric interior penalty coupling

Y. Efendiev [a,b], J. Galvis [c,*], R. Lazarov [a], M. Moon [a], M. Sarkis [d,e]

[a] Department of Mathematics, Texas A&M University, College Station, TX 77843, USA
[b] SRI-Center for Numerical Porous Media, King Abdullah University of Science and Technology (KAUST), Thuwal 23955-6900, Saudi Arabia
[c] Departamento de Matemáticas, Universidad Nacional de Colombia, Carrera 45 No. 26-85, Edificio Uriel Gutierréz, Bogotá D.C., Colombia
[d] Mathematical Sciences Department, Worcester Polytechnic Institute, 100 Institute Road, Worcester, MA 01609-2280, USA
[e] Instituto Nacional de Matemática Pura e Aplicada, Estrada Dona Castorina 110, CEP 22460-320, Rio de Janeiro, Brazil

ARTICLE INFO

Article history:
Received 27 February 2013
Received in revised form 19 July 2013
Accepted 24 July 2013
Available online 6 August 2013

Keywords:
Multiscale finite element method
Discontinuous Galerkin
Snapshot spaces
Upscaling

ABSTRACT

Motivated by applications to numerical simulations of flows in highly heterogeneous porous media, we develop multiscale finite element methods for second order elliptic equations. We discuss a multiscale model reduction technique in the framework of the discontinuous Galerkin finite element method. We propose two different finite element spaces on the coarse mesh. The first space is based on a local eigenvalue problem that uses an interior weighted L_2-norm and a boundary weighted L_2-norm for computing the "mass" matrix. The second choice is based on generation of a snapshot space and subsequent selection of a subspace of a reduced dimension. The approximation with these multiscale spaces is based on the discontinuous Galerkin finite element method framework. We investigate the stability and derive error estimates for the methods and further experimentally study their performance on a representative number of numerical examples.

1. Introduction

In this paper we present a study of numerical methods for the simulation of flows in highly heterogeneous porous media. The media properties are assumed to contain multiple scales and high contrast. In this case, solving the systems arising in the approximation of the flow equation on a fine grid that resolves all scales by the finite element, finite volume, or mixed FEM could be prohibitively expensive, unless special care is taken for solving the resulting system. A number of techniques have been proposed to efficiently solve these fine-grid systems. Among these are multigrid methods (e.g., [5,14]), multilevel methods (e.g., [32,33]), and domain decomposition techniques (e.g., [16,18,23–25,31]).

More recently, a new large class of accurate reduced-order methods has been introduced and used in various applications. These include Galerkin multiscale finite elements (e.g., [3,9,13,20–22]), mixed multiscale finite element methods (e.g., [1,2,4,27]), the multiscale finite volume method (see, e.g., [28]), mortar multiscale methods (see, e.g., [6,34]), and variational multiscale methods (see, e.g., [26]). Our main goal is to extend these concepts and to develop a systematic methodology for solving complex multiscale problems with high-contrast and no-scale separation by using discontinuous basis functions.

In this paper, we study the multiscale model reduction techniques within discontinuous Galerkin framework. As the problem is expected to be solved for many input parameters such as source terms, boundary conditions, and spatial heterogeneities, we divide the computation into two stages (following known formalism [8,30,29]): offline and online, where

* Corresponding author.
E-mail address: jcgalvisa@unal.edu.co (J. Galvis).

0021-9991/$ – see front matter
http://dx.doi.org/10.1016/j.jcp.2013.07.028

our goal in the offline stage is to construct a reduced dimensional multiscale space to be used for rapid computations in the online stage. In the offline stage [19], we generate a snapshot space and propose a local spectral problem that allows selecting dominant modes in the space of snapshots. In the online stage we use the basis functions computed offline to solve the problem for current realization of the parameters (a further spectral selection may be done in the online step in each coarse block). As a result, the basis functions generated by coarse block computations are discontinuous along the coarse-grid inter-element faces/edges. Previously, e.g. [19], in order to generate conforming basis functions, multiplication by partition of unity functions has been used. However, this procedure modifies original spectral basis functions and is found to be difficult to apply for more complex flow problems. In this paper, we propose and explore the use of local model reduction techniques within the framework of the discontinuous Galerkin finite element methods.

We introduce a Symmetric Interior Penalty Discontinuous Galerkin (SIPG) method that uses spectral basis functions that are constructed in special way in order to reduce the degrees of freedom of the local (coarse-grid) approximation spaces. Also we discuss the use of penalty parameter in the SIPG method and derive a stability result for a penalty that scales as the inverse of the fine-scale mesh. We show that the stability constant is independent of the contrast. The latter is important as the problems under consideration have high contrast.

We also derive error estimates and discuss the convergence issues of the method. Additionally, the efficacy of the proposed methods is demonstrated on a set of numerical experiments with flows in high-contrast media where the permeability fields have subregions of high conductivity, which form channels and islands. In both cases we observe that as the dimension of the coarse-grid space increases, the error decreases and the decrease is proportional to the eigenvalue that the corresponding eigenvector is not included in the coarse space. In particular, we present results when the snapshot space consists of local solutions.

The paper is organized in the following way. In Section 2, we present our model problem in a weak form and introduce the approximation method that involves two grids, fine (that resolves all scales of the heterogeneity) and coarse (where the solution will be sought). On each cell of the coarse mesh we introduce a lower dimensional space of functions that are defined on the fine mesh. We also show that the method is stable in a special DG norm. In Section 3, we present two main choices of local spaces. The first one is based on a few eigenfunctions of special spectral problems in the style of [16,23]. The second choice is based on the concept of snapshots [17]. In Section 4, we present some numerical experiments and report the error of the discontinuous Galerkin method with the constructed coarse-grid spaces and in Section 5, we discuss the numerical results. The theoretical results are derived under the assumption that the penalty stabilization depends on the fine-mesh size. Based on the numerical experiments we can conclude that the interior penalty Galerkin method gives reasonable practical results in using coarse-grid spaces generated by special problems, solved locally on each coarse-grid block, that take into account the highly heterogeneous behavior of the coefficient of the differential equation (in our case, the permeability).

2. Continuous and discrete problems

We consider the following problem: Find $u^* \in H_0^1(\Omega)$ such that

$$a(u^*, v) = f(v) \quad \text{for all } v \in H_0^1(\Omega) \tag{1}$$

where

$$a(u, v) := \int_\Omega \kappa(x)\nabla u \cdot \nabla v \, dx \quad \text{and} \quad f(v) := \int_\Omega f v \, dx.$$

Here Ω is a bounded domain in R^d, $d = 2, 3$ with polygonal boundary. We assume that $f \in L_2(\Omega)$ and the coefficient $\kappa(x)$ represents the permeability of a highly heterogeneous porous media with high contrast, that is high ratio between the maximum and minimum values, see Fig. 1. Our main goal in this paper is to develop an approximation method for (1) on a coarse grid using certain "low energy" local eigenfunctions within the discontinuous Galerkin framework.

We consider the two dimensional case. The method and results presented here extend for the three dimensional case. We split the domain Ω into disjoint polygonal subregions $\{\Omega_i\}_{i=1}^N$ of diameter $O(H_i)$ so that $\overline{\Omega} = \bigcup_{i=1}^N \overline{\Omega}_i$. We assume that the substructures $\{\Omega_i\}_{i=1}^N$ form a geometrically conforming partition of Ω. In this case, for $i \neq j$, the intersection $\partial\Omega_i \cap \partial\Omega_j$ is either empty, a vertex of Ω_i and/or Ω_j, or a common edge of $\partial\Omega_i$ and $\partial\Omega_j$.

Further, in each Ω_i we introduce a shape regular triangulation $\mathcal{T}_h(\Omega_i)$ with triangular elements and maximum mesh size h_i. The resulting triangulation of Ω is in general nonmatching across $\partial\Omega_i$. Let $X_h(\Omega_i)$ be the regular finite element space of piecewise linear and continuous functions in $\mathcal{T}_h(\Omega_i)$. We do not assume that functions in $X_h(\Omega_i)$ vanish on $\partial\Omega_i \cap \partial\Omega$. We define

$$X_h(\Omega) = X_h(\Omega_1) \times \cdots \times X_h(\Omega_N)$$

and represent functions v of $X_h(\Omega)$ as $v = \{v_i\}_{i=1}^N$ with $v_i \in X_h(\Omega_i)$. For simplicity, we also assume that the permeability $\kappa(x)$ is constant over each fine-grid element.

Due to the fact that $\mathcal{T}_h(\Omega_i)$ and $\mathcal{T}_h(\Omega_j)$ are independent from each other on a common edge $E = \partial\Omega_i \cap \partial\Omega_j$ they may introduce two different partitions of E which are merged to obtain a set of faces $E_{ij} \subset E$. Since the functions in $X_h(\Omega)$ are discontinuous along the interfaces, it is necessary to distinguish between $E \subset \overline{\Omega}_i$ and $E \subset \overline{\Omega}_j$. From now on the Ω_i-side of E will be denoted by E_{ij} while on the Ω_j-side of E will be denoted by E_{ji}. Geometrically, E_{ij} and E_{ji} are the same object.

We use the following harmonic averages along the edges E_{ij}. For $i, j \in \{1, \ldots, N\}$ define

$$\kappa_{ij} = \frac{2\kappa_i\kappa_j}{\kappa_i + \kappa_j} \quad \text{and} \quad h_{ij} = \frac{2h_ih_j}{h_i + h_j}. \tag{2}$$

Note, that the functions κ_{ij} and h_{ij} are piecewise constants over the edge E_{ij} on a mesh that is obtained by merging the partitions $\mathcal{T}_h(\Omega_i)$ and $\mathcal{T}_h(\Omega_j)$ along their common edge E_{ij}.

The discrete problem obtained by the DG method, see [7,12] is: Find $u_h^* = \{u_{h,i}^*\}_{i=1}^N \in X_h(\Omega)$, $u_{h,i}^* \in X_h(\Omega_i)$, such that

$$a_h^{DG}(u_h^*, v_h) = f(v_h) \quad \text{for all } v_h = \{v_{h,i}\}_{i=1}^N \in X_h(\Omega), \tag{3}$$

where $a_h^{DG}(u_h, v_h)$, defined on $X_h(\Omega) \times X_h(\Omega)$, and $f(v)$, defined on $X_h(\Omega)$, are given by

$$a_h^{DG}(u, v) = \sum_{i=1}^N a_i^{DG}(u, v) \quad \text{and} \quad f(v) = \sum_{i=1}^N \int_{\Omega_i} f v_i \, dx. \tag{4}$$

Here, each local bilinear form a_i^{DG} is given as a sum of three symmetric bilinear forms:

$$a_i^{DG}(u, v) := a_i(u, v) + s_i(u, v) + p_i(u, v), \tag{5}$$

where a_i is the bilinear form associated with the "energy",

$$a_i(u, v) := \int_{\Omega_i} \kappa(x) \nabla u_i \cdot \nabla v_i \, dx, \tag{6}$$

the s_i is the bilinear form ensuring consistency and symmetry

$$s_i(u, v) := \sum_{E_{ij} \subset \partial\Omega_i} \frac{1}{l_{ij}} \int_{E_{ij}} \kappa_{ij} \left(\frac{\partial u_i}{\partial n_i}(v_j - v_i) + \frac{\partial v_i}{\partial n_i}(u_j - u_i) \right) ds, \tag{7}$$

and p_i is the penalty bilinear form that is added for stability

$$p_i(u, v) := \sum_{E_{ij} \subset \partial\Omega_i} \frac{1}{l_{ij}} \frac{\delta}{h_{ij}} \int_{E_{ij}} \kappa_{ij}(u_j - u_i)(v_j - v_i) \, ds. \tag{8}$$

Here κ_{ij} is defined in (2) and $\frac{\partial}{\partial n_i}$ denotes the outward normal derivative on $\partial\Omega_i$. The parameter δ is a positive penalty parameter. In order to simplify notation we included the index $j = \partial$ in the definition of the bilinear forms s_i and p_i above. In order to include $E_{i\partial} := \partial\Omega_i \cap \partial\Omega$ in the summation sing, we set $l_{ij} = 2$ when $i, j \neq \partial$ and $l_{ij} = 1$ when $j = \partial$. We also let $v_\partial = 0$ for all $v \in X_h(\Omega)$, and define $\kappa_{i\partial} = \kappa_i$ and $h_{i\partial} = h_i$. We note that when κ_{ij} is given by the harmonic average, then $\min\{\kappa_i, \kappa_j\} \leqslant \kappa_{ij} \leqslant 2\min\{\kappa_i, \kappa_j\}$.

For later use we define the positive bilinear forms d_i as

$$d_i(u, v) = a_i(u, v) + p_i(u, v), \tag{9}$$

and the broken bilinear form d_h for $X_h(\Omega)$:

$$d_h(u, v) := \sum_{i=1}^N d_i(u, v). \tag{10}$$

For $u = \{u_i\}_{i=1}^N \in X_h(\Omega)$ the associated broken norm is then defined by

$$\|u\|_{h,\delta}^2 = d_h(u, u) = \sum_{i=1}^N \left\{ \|\kappa_i^{1/2} \nabla u_i\|_{L^2(\Omega_i)}^2 + \sum_{E_{ij} \subset \partial\Omega_i} \frac{1}{l_{ij}} \frac{\delta}{h_{ij}} \int_{E_{ij}} \kappa_{ij}(u_i - u_j)^2 \, ds \right\}. \tag{11}$$

We also have the following lemma shown in [12, Lemma 3.1]. Here we provide a sketch of the proof for the sake of completeness.

Lemma 2.1. *There exists $\delta_0 > 0$ such that for $\delta \geqslant \delta_0$ and for all $u \in X_h(\Omega)$ the following inequalities hold*:

$$\gamma_0 d_i(u,u) \leqslant a_i^{DG}(u,u) \leqslant \gamma_1 d_i(u,u), \quad i = 1,\dots,N, \tag{12}$$

and

$$\gamma_0 d_h(u,u) \leqslant a_h^{DG}(u,u) \leqslant \gamma_1 d_h(u,u), \tag{13}$$

where γ_0 and γ_1 are positive constants independent of the κ_i, h_i, H_i and u.

Proof. First, we want to prove that $\gamma_0 d_i(u,u) \leqslant a_i^{DG}(u,u)$. Since $a_i^{DG}(u,u) = a_i(u,u) + s_i(u,u) + d_i(u,u)$, the proof reduces to bound $|s_i(u,u)|$. Note that

$$s_i(u,u) = 2\sum_{E_{ij}\subset\partial\Omega_i} \frac{1}{l_{ij}} \int_{E_{ij}} \kappa_{ij} \frac{\partial u_i}{\partial n_i}(u_j - u_i) = 2\sum_{E_{ij}\subset\partial\Omega_i} \frac{1}{l_{ij}} I_{ij}$$

where we have defined $I_{ij} := \int_{E_{ij}} \kappa_{ij} \frac{\partial u_i}{\partial n_i}(u_j - u_i)\,ds$. We have

$$I_{ij} \leqslant \left\|\kappa_{ij}^{1/2}\nabla u_i\right\|_{L^2(E_{ij})} \left\|\kappa_{ij}^{1/2}(u_j - u_i)\right\|_{L^2(E_{ij})}. \tag{14}$$

Using the following inequality for $u_i \in X_h(\Omega_i)$

$$h_i \left\|\kappa_{ij}^{1/2}\nabla u_i\right\|^2_{L^2(E_{ij})} \leqslant C \left\|\kappa_i^{1/2}\nabla u_i\right\|^2_{L^2(\Omega_i)}, \tag{15}$$

the Young inequality with arbitrary $\epsilon > 0$ and the fact $h_{ij} \leqslant 2h_i$, we get

$$I_{ij} \leqslant C\left\{\epsilon \left\|\kappa_i^{1/2}\nabla u_i\right\|^2_{L^2(\Omega_i)} + \frac{1}{4\epsilon}\frac{1}{2h_{ij}} \left\|\kappa_{ij}^{1/2}(u_j - u_i)\right\|^2_{L^2(E_{ij})}\right\}. \tag{16}$$

Then, multiplying by $1/l_{ij}$ and summing over the edges $E_{ij} \subset \Omega_i$, we get

$$\left|s_i(u,u)\right| \leqslant 2CN_E\epsilon \left\|\kappa_i^{1/2}\nabla u_i\right\|^2_{L^2(\Omega_i)} + \frac{C}{4\epsilon} \sum_{E_{ij}\subset\partial\Omega_i} \frac{1}{l_{ij}}\frac{1}{h_{ij}} \left\|\kappa_{ij}^{1/2}(u_j - u_i)\right\|^2_{L^2(E_{ij})} \tag{17}$$

$$= 2CN_E\epsilon a_i(u,u) + \frac{C}{4\epsilon\delta} p_i(u,u). \tag{18}$$

Here N_{CE} denotes the number of *coarse edges* of subdomain Ω_i (for instance, $N_{CE} = 4$ if the coarse subdomains have rectangular shape). Choosing $\epsilon = 1/(4CN_{CE})$ we get

$$\left|s_i(u,u)\right| \leqslant 0.5 a_i(u,u) + \frac{C^2 N_{CE}}{\delta} p_i(u,u)$$

and then

$$0.5 a_i(u,u) + \left(1 - \frac{C^2 N_{CE}}{\delta}\right) p_i(u,u) \leqslant a^{DG}(u,u) \leqslant 1.5 a_i(u,u) + \left(1 + \frac{C^2 N_{CE}}{\delta}\right) p_i(u,u). \tag{19}$$

Therefore the result holds if we take $\delta \geqslant \delta_0 > C^2 N_{CE}$, $\gamma_0 = \min\{0.5, 1 - (C^2 N_{CE})/\delta\}$ and $\gamma_1 = \max\{1.5, (C^2 N_{CE})/\delta\}$. □

Remark 2.2. We note that γ_1/γ_0 in Lemma 2.1 deteriorates when δ gets larger. In practice, however, $\delta \geqslant \delta_0$ is chosen such that $\delta = O(1)$, therefore, from now on we assume that all the estimates will not depend on δ.

3. Coarse-grid spaces

In this section, we will construct local multiscale basis functions. We will follow GMsFEM where one needs the snapshot space, see [17,15]. In this snapshot space, local spectral problems are designed and solved to compute multiscale basis functions. To keep our presentation simple, we first use the snapshot space to be fine-grid functions within a coarse region. Thus, the local spectral problems will be posed on the fine grid. Next, we will discuss how a general snapshot space can be used.

3.1. Fine-grid snapshot space and amended eigenvalue problem

Following [20,15], we consider the eigenvalue problem in Ω_i for the eigenvalues $\lambda^I_{i,\ell}$ and the eigenfunctions $\psi^I_{i,\ell}(x)$:

$$-\mathrm{div}\big(\kappa(x)\nabla\psi^I_{i,\ell}\big) = \lambda^I_{i,\ell}\widetilde{\kappa}\psi^I_{i,\ell}, \quad x\in\Omega_i, \qquad \kappa(x)\nabla\psi^I_{i,\ell}\cdot n = 0, \quad x\in\partial\Omega_i, \tag{20}$$

where n is the outer unit normal vector to $\partial\Omega_i$ and $\widetilde{\kappa}$ is a properly selected weight; for scalar permeability, we select $\widetilde{\kappa}=\kappa$ while for tensor permeability we refer to [20]. The super-index I is used to distinguish from the other method we develop here (with index II).

The eigenvalue problem considered above is solved in a discrete setting. A modification of this eigenvalue problem is needed in order to be able to bound terms involving integral of functions over boundary of subdomains. We also mention that, the modified eigenvalue problem introduced next is motivated by the error analysis developed below in Section 3.4. More precisely, for any given subdomain Ω_i, we find $\lambda^I_{i,\ell}$ and $\psi^I_{i,\ell}\in X_h(\Omega_i)$ such that

$$a_i\big(\psi^I_{i,\ell},z\big) = \lambda_{i,\ell}\big(m_i\big(\psi^I_{i,\ell},z\big)+m^\delta_i\big(\psi^I_{i,\ell},z\big)\big) \quad \text{for all } z\in X_h(\Omega_i). \tag{21}$$

Here, a_i is defined in (6), the bilinear form $m_i(\cdot,\cdot)$ is defined by

$$m_i(v,z) = \int_{\Omega_i}\kappa vz, \tag{22}$$

and the (boundary) bilinear form $m^\delta_i(\cdot,\cdot)$ is given by

$$m^\delta_i(v,z) = \sum_{E_{ij}\subset\partial\Omega_i}\frac{1}{l_{ij}}\frac{\delta}{h_{ij}}\int_{E_{ij}}\kappa_{ij}vz\,ds. \tag{23}$$

These eigenvalue problems allow us to obtain simple error estimates since the eigenvectors can approximate fine-grid functions simultaneously in a norm that includes interior weighted semi-norm in the coarse-grid block and weighted L^2-norm on the interfaces.

We order the eigenvalues so that $0\leqslant\lambda^I_{i,1}\leqslant\lambda^I_{i,2}\leqslant\cdots\leqslant\lambda^I_{i,N_i}$, where N_i is the number of vertices of $\mathcal{T}_h(\Omega_i)$, i.e., the number of degrees of freedom associated to $X_h(\Omega_i)$. Then, in each subdomain Ω_i, we take the L_i eigenfunctions corresponding to the smallest eigenvalues and use them as the multiscale basis. More precisely, define

$$X^I_H(\Omega_i) := \mathrm{span}\big\{\psi^I_{i,\ell}, 1\leqslant l\leqslant L_i\big\}\subset X_h(\Omega_i), \quad i=1,\ldots,N.$$

Finally, the coarse space is defined as

$$X^I_H(\Omega) := X^I_H(\Omega_1)\times\cdots\times X^I_H(\Omega_N)\subset X_h(\Omega).$$

We refer to $X^I_H(\Omega)$ as a spectral coarse space due to its construction.

Now the coarse-grid problem is to find $u^{ms,I}_H\in X^I_H(\Omega)$ such that

$$a^{DG}_h\big(u^{ms,I}_H,v_H\big) = f(v_H) \quad \text{for all } v_H\in X_H(\Omega). \tag{24}$$

Note that the dimension of $X^I_H(\Omega)$ depends on the number of eigenvectors chosen in each coarse block Ω_i. An ideal situation would be when small number of eigenvectors in Ω_i represent (approximate) the restriction of the solution to that subdomain accurately.

Remark 3.1 *(On the original weighted eigenvalue problem).* We refer to the eigenvalue problem (21) as "amended eigenvalue problem" due to the introduced modification on the right hand side. This modification is done with respect to the simpler eigenvalue problem

$$a_i\big(\psi^I_{i,\ell},z\big) = \lambda^I_{i,\ell}m_i\big(\psi^I_{i,\ell},z\big) \quad \text{for all } z\in X_h(\Omega_i). \tag{25}$$

We refer to this eigenvalue problem as (original) weighted eigenvalue problem. Although the convergence of the method using this simpler eigenvalue problem is not guarantee by our analysis, the resulting method was tested numerically where we observed also good results in comparison with the amended eigenvalue problem. See Section 4.

3.2. General snapshot space and an example

In general, one can consider a general snapshot space for solving local eigenvalue problems. As we discussed in the Introduction, the use of general snapshot space can have an advantage when additional information is known about the local solution space. The subset of all possible functions that satisfy the known properties of the solution space can be taken as the snapshot space. In this way we solve eigenvalue problem on more relevant (smaller dimension) subspaces instead of the space of fine degrees of freedom. For example, if solutions need to be computed only for a subspace of possible source terms, one can restrict the snapshot space to the space of local solutions for those sources and do not consider all fine-grid functions. To demonstrate that it is possible to use a snapshot space strictly smaller than $X_h(\Omega)$, we consider an example where the snapshot space consists of all local solutions of the homogeneous equation with boundary conditions restriction on the boundary of the finite element nodal basis functions (or the set of all discrete a_i-harmonic functions in each block). More precisely, for the nodal basis function $\delta_k(x)$ corresponding to the k-th node on $\partial\Omega_i$, we consider the problem

$$-\operatorname{div}(\kappa\nabla\phi_{i,k}) = 0 \quad \text{in } \Omega_i, \qquad \phi_{i,k} = \delta_k \quad \text{on } \partial\Omega_i. \tag{26}$$

The $\phi_{i,k} \in X_h(\Omega_i)$, $k = 1, \dots, M_i$, is the (finite element) solution of this local problem. Here M_i denotes the number of nodal basis function corresponding to nodes on $\partial\Omega_i$. Then the snapshot space is defined by

$$X_h^{\text{snap}}(\Omega_i) = \operatorname{span}\{\phi_{i,k}, 1 \leqslant k \leqslant M_i\}, \quad i = 1, \dots, N. \tag{27}$$

Remark 3.2. Here, the reference solution we want to approximate on a coarse grid is the Galerkin projection of u_h^*, solution of (3), into the global snapshot space $X_h^{\text{snap}}(\Omega) = X_h^{\text{snap}}(\Omega_1) \times \cdots \times X_h^{\text{snap}}(\Omega_N)$.

Our objective is to construct a possibly smaller dimension space $X_H^{\text{snap}}(\Omega_i)$ which is a subspace of $X_h^{\text{snap}}(\Omega_i)$. The construction is done using an appropriate spectral decomposition. For this, we define the matrices

$$A_i^{\text{snap}} = \left[a_i(\phi_{i,k}, \phi_{i,k'})\right]_{k,k'=1}^{M_i} \quad \text{and} \quad M_i^{\text{snap}} = \left[m_i^{\delta}(\phi_{i,k}, \phi_{i,k'})\right]_{k,k'}^{M_i}$$

and solve the following algebraic eigenvalue problem

$$A_i^{\text{snap}}\alpha_{i,\ell} = \lambda_{i,\ell}^{\text{snap}} M_i^{\text{snap}}\alpha_{i,\ell}. \tag{28}$$

We write $\alpha_{i,\ell} = (\alpha_{i,\ell;1}, \dots, \alpha_{i,\ell;M_i}) \in \mathbb{R}^{M_i}$ and define the corresponding finite element functions, $\psi_{i,\ell}^{II} \in X_h(\Omega_i)$ as

$$\psi_{i,\ell}^{II} = \sum_{k=1}^{M_i} \alpha_{i,\ell;k}\phi_{i,k}, \quad \ell = 1, \dots, M_i.$$

Note that the matrices A_i^{snap} and M_i^{snap} are computed in the space of snapshots in Ω_i. Assume that $0 \leqslant \lambda_{i,1}^{\text{snap}} \leqslant \cdots \leqslant \lambda_{i,M_i}^{\text{snap}}$, and choose the L_i eigenvectors $\psi_{i,1}^{II}, \dots, \psi_{i,L_i}^{II}$ that correspond to the smallest L_i eigenvalues. We introduce

$$X_H^{II}(\Omega_i) = \operatorname{span}\left\{\psi_{i,\ell}^{II}\colon\ l = 1, \dots, L_i\right\} \quad \text{for } i = 1, \dots, N$$

and define the global coarse space by

$$X_H^{II}(\Omega) := X_H^{II}(\Omega_1) \times \cdots \times X_H^{II}(\Omega_N) \subset X_h(\Omega).$$

The coarse problem is to find $u_H^{ms,II} \in X_H^{II}(\Omega)$ such that

$$a_h^{DG}\left(u_H^{ms,II}, v_H\right) = f(v_H) \quad \text{for all } v_H \in X_H^{II}(\Omega). \tag{29}$$

Remark 3.3. Note that, according to the definition of m_i^{δ} in (23), the matrix M_i^{snap} scales with $1/h_{ij}$. Then, the resulting eigenvalues scale with h_{ij} while the eigenspaces do not depend on h_{ij}. A similar situation is also valid for Method II and the eigenvalue problem (21). It is easy to see from our main Theorem 3.6 (stated and proved below) that this scaling does not affect the convergence rate with respect to the number of eigenvectors used in the coarse space.

Remark 3.4. Instead of the M_i^{snap} defined above, we can use

$$M_i^{\text{snap}} = \left[m_i(\phi_{i,k}, \phi_{i,k'}) + m_i^{\delta}(\phi_{i,k}, \phi_{i,k'})\right]_{k,k'=1}^{M_i}.$$

3.3. Stability estimate

In this subsection, we present a best approximation result for the coarse-grid solution.

Lemma 3.5. *Let $u_h^* \in X_h(\Omega)$ and $u_H^{ms,I} \in X_H^I(\Omega)$ be the solutions of (1) and (24), correspondingly. We have*

$$d_h\big(u_h^* - u_H^{ms,I}, u_h^* - u_H^{ms,I}\big) \leqslant C_1 d_h\big(u_h^* - v, u_h^* - v\big) \quad \text{for all } v \in X_H^I(\Omega) \tag{30}$$

with C_1 independent of κ_i, h_i, H_i, u_h^* and $u_H^{ms,I}$.

Proof. For all $v \in X_H^I(\Omega)$,

$$a_h^{DG}\big(u_h^*, v\big) = f(v) \quad \text{and} \quad a_h^{DG}\big(u_H^{ms,I}, v\big) = f(v). \tag{31}$$

Then $a_h^{DG}(u_h^* - u_H^{ms,I}, v) = 0$ and since $u_H^{ms,I} \in X_H^I(\Omega)$,

$$a_h^{DG}\big(u_h^* - u_H^{ms,I}, u_h^* - u_H^{ms,I}\big) = a_h^{DG}\big(u_h^* - u_H^{ms,I}, u_h^* - v\big). \tag{32}$$

Using a Cauchy–Schwarz inequality and (13) in Lemma 2.1,

$$\gamma_0 d_h\big(u_h^* - u_H^{ms,I}, u_h^* - u_H^{ms,I}\big) \leqslant a_h^{DG}\big(u_h^* - u_H^{ms,I}, u_h^* - u_H^{ms,I}\big) = a_h^{DG}\big(u_h^* - u_H^{ms,I}, u_h^* - v\big) \tag{33}$$

$$\leqslant a_h^{DG}\big(u_h^* - u_H^{ms,I}, u_h^* - u_H^{ms,I}\big)^{1/2} a_h^{DG}\big(u_h^* - v, u_h^* - v\big)^{1/2} \tag{34}$$

$$\leqslant \gamma_1 d_h\big(u_h^* - u_H^{ms,I}, u_h^* - u_H^{ms,I}\big)^{1/2} d_h\big(u_h^* - v, u_h^* - v\big)^{1/2}. \tag{35}$$

Taking $C_1 = (\gamma_1/\gamma_0)^2$, we get

$$d_h\big(u_h^* - u_H^{ms,I}, u_h^* - u_H^{ms,I}\big) \leqslant C_1 d_h\big(u_h^* - v, u_h^* - v\big) \tag{36}$$

and this completes the proof. □

Analogous best approximation results, with respect to the fine-grid reference solutions, hold true for the coarse problem (29) and even for the coarse problem of the method using the original weighted eigenvalue problem (see Remark 3.1).

3.4. Error estimates in terms of the local energy captured

The following theorem gives an error estimates with respect to the number of eigenvectors used. Therefore, we obtain convergence to the reference solution when we add more and more eigenvectors to the coarse space. The error estimates are written in terms of the amount of local energy (of the reference solution) that is captured using the selected eigenmodes.

Theorem 3.6. *Let u_h^* and $u_H^{ms,I}$ be the solution of the problem (3) and (24), respectively. Put $u_h^* = \{u_i^*\}_{i=1}^N$. In each subdomain we can write*

$$u_i^* = \sum_{\ell=1}^{N_i} c_\ell\big(u_i^*\big)\psi_{i,\ell}^I \quad \text{and} \quad a_i\big(u_i^*, u_i^*\big) = \sum_{\ell=1}^{N_i} \lambda_{i,\ell}^I c_\ell\big(u_i^*\big)^2,$$

where $c_\ell(u_i^*) = m_i(u_i^*, \psi_{i,\ell}^I) + m_i^\delta(u_i^*, \psi_{i,\ell}^I)$. The following error estimate holds

$$d_h\big(u_h^* - u_H^{ms,I}, u_h^* - u_H^{ms,I}\big) \leqslant C_1\left(1 + \frac{4}{\min_{1\leqslant i\leqslant N} \lambda_{i,L_i+1}^I}\right) \sum_{i=1}^{N} \sum_{\ell=L_i+1}^{N_i} \lambda_{i,\ell}^I c_\ell\big(u_i^*\big)^2.$$

Proof. Using the truncated expansion of solutions, define the interpolation $I^H(u_h^*)$ by

$$I^H\big(u_h^*\big) = \big\{I_i^H\big(u_i^*\big)\big\}_{i=1}^N \quad \text{where } I_i^H\big(u_i^*\big) = \sum_{\ell=1}^{L_i} c_\ell\big(u_i^*\big)\psi_{i,\ell}^I,$$

where $c_\ell(u_i^*) = m_i(u_i^*, \psi_{i,\ell}^I) + m_i^\delta(u_i^*, \psi_{i,\ell}^I)$, $i = 1, \ldots, N$. Note that $I_i^H(u_i^*)$ is the projection of u_i^* into the space spanned by the first L_i eigenvectors. Now we take $v = I^H(u_h^*)$ in Lemma 3.5 to obtain

$$d_h\big(u_h^* - u_H^{ms,I}, u_h^* - u_H^{ms,I}\big) \leqslant C_1 d_h\big(u_h^* - I^H\big(u_h^*\big), u_h^* - I^H\big(u_h^*\big)\big) = d_h(e, e), \tag{37}$$

where we have defined $e = \{e_i\}_{i=1}^N$ with

$$e_i = u_i^* - I_i^H(u_i^*) = \sum_{\ell=L_i+1}^{N_i} c_\ell(u_i^*)\psi_{i,\ell}^I.$$

Now we bound $d_h(e,e)$. First, we observe that

$$d_h(e,e) = \sum_{i=1}^N \big(a_i(e_i,e_i) + p_i(e,e)\big). \tag{38}$$

The second term in this sum can be bounded as follows. We write

$$p_i(e,e) = \sum_{E_{ij}\subset\delta\Omega_i} \frac{1}{l_{ij}}\frac{\delta}{h_{ij}}\int_{E_{ij}} \kappa_{ij}(e_j - e_i)^2\,ds \tag{39}$$

$$\leqslant 2\sum_{E_{ij}\subset\partial\Omega_i}\left(\frac{1}{l_{ij}}\frac{\delta}{h_{ij}}\int_{E_{ij}}\kappa_{ij}(e_j)^2\,ds + \frac{1}{l_{ij}}\frac{\delta}{h_{ij}}\int_{E_{ij}}\kappa_{ij}(e_i)^2\,ds\right) \tag{40}$$

$$\leqslant 2\sum_{E_{ij}\subset\partial\Omega_i}\frac{1}{l_{ij}}\frac{\delta}{h_{ij}}\int_{E_{ij}}\kappa_{ij}(e_j)^2\,ds + 2m_i^\delta(e_i,e_i). \tag{41}$$

Adding over all subdomains we get

$$\sum_{i=1}^N p_i(e,e) \leqslant 2\sum_{i=1}^N\sum_{E_{ij}\subset\partial\Omega_i}\frac{1}{l_{ij}}\frac{\delta}{h_{ij}}\int_{E_{ij}}\kappa_{ij}(e_i)^2\,ds + 2\sum_{i=1}^N m_i^\delta(e_i,e_i)$$

$$= 4\sum_{i=1}^N m_i^\delta(e_i,e_i). \tag{42}$$

On the other hand, if we use the increasing order of eigenvalues of the eigenvalue problem (21), we get

$$m_i^\delta(e_i,e_i) \leqslant m_i(e_i,e_i) + m_i^\delta(e_i,e_i) \leqslant \frac{1}{\lambda_{i,L_i+1}^I}a_i(e_i,e_i) \tag{43}$$

which, together with (38) and (42), gives

$$\sum_{i=1}^N \big(a_i(e_i,e_i) + p_i(e,e)\big) \leqslant \sum_{i=1}^N \big(a_i(e_i,e_i) + 4m_i^\delta(e_i,e_i)\big) \tag{44}$$

$$= \sum_{i=1}^N\left(1 + \frac{4}{\lambda_{i,L_i+1}^I}\right)\sum_{\ell=L_i+1}^{N_i}\lambda_{i,\ell}^I c_\ell(u_i^*)^2 \tag{45}$$

$$\leqslant \left(1 + \frac{4}{\min\limits_{1\leqslant i\leqslant N}\lambda_{i,L_i+1}^I}\right)\sum_{i=1}^N\sum_{\ell=L_i+1}^{N_i}\lambda_{i,\ell}^I c_\ell(u_i^*)^2. \tag{46}$$

This completes the proof. □

Remark 3.7. Using our analysis, in order to obtain further bounds for the error we have to study the convergence of the sum $\sum_{\ell=1}^{N_i}\lambda_{i,\ell}^I c_\ell(u_i^*)^2$ (that is, the decay of the coefficients $c_\ell(u_i^*)^2$ with increasing ℓ). This can depend on the smoothness of the solution and it will be a subject of future research.

Remark 3.8. A similar result holds for the method constructed with snapshot space presented in Section 3.2. In this case the reference solution is the solution obtaining by a Galerkin projection on the snapshot space. See Remark 3.2.

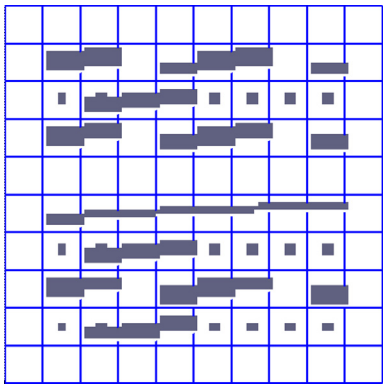

Fig. 1. High-contrast coefficient. Example 1.

4. Numerical experiments

In this section we present representative numerical experiments. In particular, we compute the coarse (or upscaled) solution and study the error with respect to the reference solution (or the fine-grid solution of (3)). We choose $\delta = 4$ for all the numerical tests presented here. We note that the solution of (3) depends on both fine-scale and coarse-scale parameters, h and H. We are mainly interested on the convergence (to the reference solution) when we sequentially add more and more basis functions. We study the error behavior due to the addition of coarse basis functions for fixed value of h and H.

We consider the domain $\Omega = (0,1)^2$ and divide Ω into $N = M \times M$ square coarse blocks, $\{\Omega_i\}_{i=1}^N$, which are unions of fine elements. In this case $H = 1/M$ is the coarse mesh parameter. Inside each subdomain Ω_i we generate a structured triangulation with m subintervals in each coordinate direction (and thus $h = 1/(Mm)$ is the fine mesh parameter). We consider the solution of Eq. (3) with $f = 1$ and a high-contrast coefficient described in Fig. 1. This coefficient is one in the white background and the value η in the gray regions representing high-contrast channels and high-contrast inclusions. Thus, the η represents the contrast of the media, namely the ratio of the maximum and minimum values of $\kappa(x)$.

In the following we compute the norm of the error $e = u_h^* - u_H$ between the fine-scale solution obtained by solving (3) and the coarse-grid solution u_H, which is one of the following coarse-grid functions: 1. $u_H^{ms,I}$ solution of (24) (with original eigenvalue problem and also with amended eigenvalue problem) or 2. $u_H^{ms,II}$ the solution of (29). The square of the total error is computed as $\|e\|_{h,1}^2$ where $\|\cdot\|_{h,\delta}^2$ defined in (11). The relative error is computed as $\|e\|_{h,1}^2/\|u_h^*\|_{h,1}^2$. The error is divided into two quantities, interior error and interface error. We also compute the energy error. The precise definitions are:

- *Interior Error*: (square of the) broken H^1-semi-norm of the error

$$\sum_{i=1}^{N} a_i(e,e) = \sum_{i=1}^{N} \left\| \kappa_i^{1/2} \nabla e_i \right\|_{L^2(\Omega_i)}^2.$$

- *Interface Error*: (square of the) L^2-norm of the jump of the error across the edges

$$\sum_{i=1}^{N} \sum_{E_{ij} \subset \partial\Omega_i} \frac{1}{l_{ij}} \frac{1}{h_{ij}} \int_{E_{ij}} \kappa_{ij} (e_i - e_j)^2.$$

- *Energy error*: (square of the) DG bilinear form, that is, $a_h^{DG}(e,e)$.

4.1. Fine-grid snapshot space and original eigenvalue problem

In this subsection, we present the numerical experiments for the method that uses the original weighted eigenvalue problem. We recall that the convergence of this method is not covered by our analysis. We numerically show the error obtained when the dimension of the coarse space is increased.

First, we recall that for high-contrast problems we include the eigenvectors corresponding to small eigenvalues (that asymptotically vanish as the contrast increases). We denote by L_i^{small} the number of these small eigenvalues in Ω_i. To see the effect of adding more basis functions, we select additional L_i^{add} eigenvalues so the total number of eigenvalues selected in the block Ω_i is $L_i^{small} + L_i^{add}$. We show that the error decays as L_i^{add} increases. For the coefficient $\kappa(x)$ and the coarse mesh shown in Fig. 1 there is only one such and eigenvalue in each coarse-grid block Ω_i and therefore $L_i^{small} = 1$, $i = 1, 2, \ldots, N$. Fig. 2 illustrates the effect of using an increasing number of eigenvectors in the solution. We show the fine-scale solution and coarse-scale solutions computed with three different coarse spaces $L_i^{add} = 0, 2, 11$.

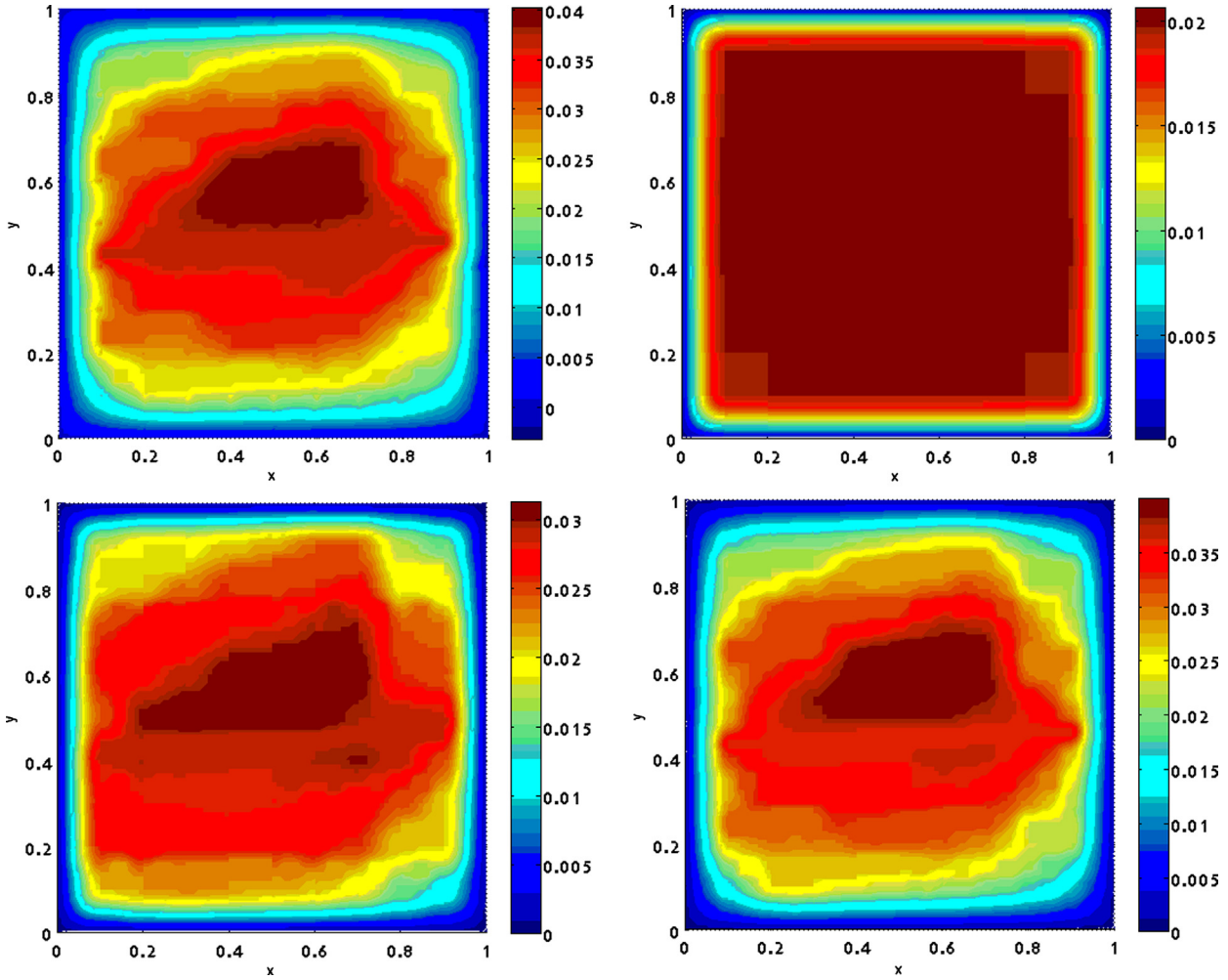

Fig. 2. Illustration of fine and coarse solutions. Fine-scale solution u_h^* (top left). Coarse-scale solution $u_H^{ms,l}$ with $L_i^{add} = 0$ eigenvalues (top right). Coarse-scale solution $u_H^{ms,l}$ with $L_i^{add} = 3$ eigenvalues (bottom left). Coarse-scale solution $u_H^{ms,l}$ with $L_i^{add} = 11$ eigenvalues (bottom right).

Table 1
Numerical results using the original weighted eigenvalue problem in Remark 3.1. Here, $h = 1/100$, $H = 1/10$, $\eta = 10^4$, and $\eta = 10^6$ (in parentheses). "Dim." stands for the dimension of the coarse space.

L_i^{add}	Dim.	Interface error	Interior error	Total error	$\lambda_{\min}$
0	100 (100)	0.026 (0.026)	0.326 (0.326)	0.3522 (0.3522)	689.4 (689.3)
2	300 (300)	0.031 (0.032)	0.221 (0.220)	0.2523 (0.2516)	1562.2 (1561.7)
4	500 (500)	0.028 (0.029)	0.171 (0.170)	0.1991 (0.1984)	2607.5 (2607.0)
6	700 (700)	0.027 (0.027)	0.133 (0.131)	0.1600 (0.1581)	5199.4 (5199.3)
8	900 (900)	0.026 (0.027)	0.114 (0.113)	0.1399 (0.1392)	7237.9 (7237.6)
10	1100 (1100)	0.025 (0.025)	0.104 (0.103)	0.1293 (0.1283)	9509.1 (9509.0)

The results for the computation of interior and interface errors are presented in Table 1 for $h = 1/100$ and $H = 1/10$ and two different contrasts. In this table, we also report the dimension of the coarse spaces (designated by "Dim.") and the number of eigenvectors that are added for each subdomain to form the coarse space. The convergence with respect to the minimum left out eigenvalue is shown in Fig. 3. In this case, we solve a 100 dimension local eigenvalue problem in each coarse block. From the results we see a convergence to the reference solution (fine-grid solution). We also observe error decay proportional to the minimum left out eigenvalue across all coarse blocks. In particular, for $H = 1/10$, we only need 3 or 4 additional functions to get an interior error or the order of 17%. This error is computed with respect to the fine-grid solution with the fine-grid mesh size $h = 1/100$. Note that, in this case, we have the total of four or five basis functions per subdomain which is comparable to the number of degrees of freedom of a classical DG method on the coarse grid.

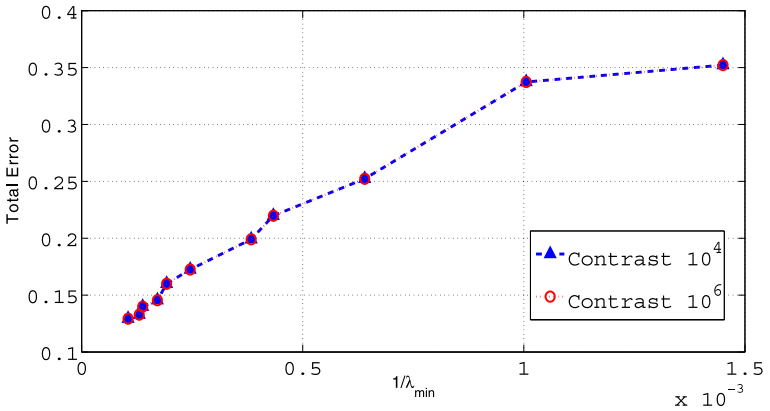

Fig. 3. Total error of Method I (in Section 3.1) vs. $1/\lambda_{min}$. Here $h = 1/100$ and the contrast is 10^6. Coarse mesh size $H = 1/10$ and contrast 10^4 and 10^6.

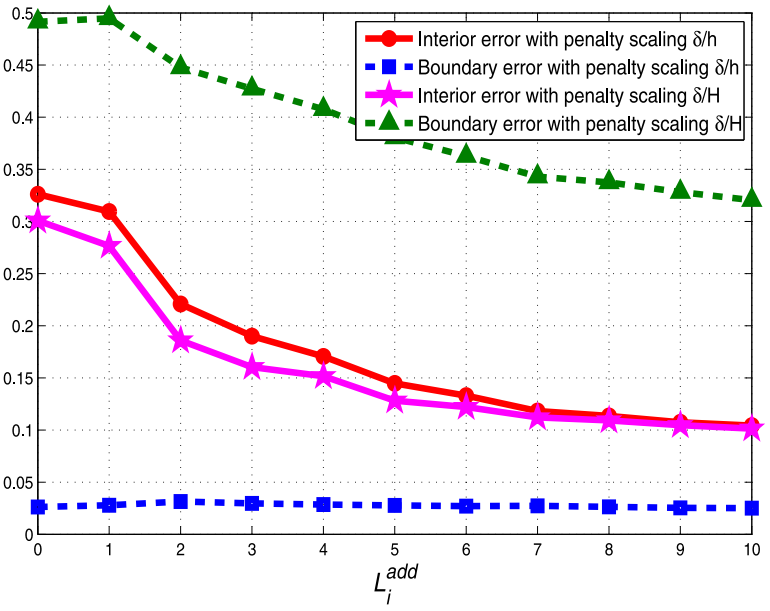

Fig. 4. The error for values of $L_i^{add} = 0, 1, \ldots, 10$ and two different penalty scalings: $\frac{\delta}{h}$ and $\frac{\delta}{H}$. Here $h = 1/100$, $H = 1/10$, and $\eta = 10^4$.

4.2. Error vs. coarse problem penalty scaling

Next, we test the error when we change the scaling of the penalty. We recall that the fine-scale problem in (3) uses a penalty term scaled by $\delta \frac{1}{l_{ij}} \frac{1}{h_{ij}}$. In the classical SIPG formulation on the coarse grid one uses a penalty scaled by $\delta \frac{1}{l_{ij}} \frac{1}{H}$. Here we experiment by computing the coarse solutions with several penalties in the range from $1/H$ to $1/h$ to identify a good penalty parameter for the coarse problem.

For this experiment we set the contrast $\eta = 10^4$, $M = 10$, $n_i = 10$, $i = 1, \ldots, N$ (and thus $H = 1/10$ and $h = 1/100$). Then, recalling that $\delta = 4$ for the numerical experiments, we have $\delta \frac{1}{H} = 40$ and $\delta \frac{1}{h_{ij}} = 400$. For these two choices of the penalty in Fig. 4 we show the decay of the interior and interface error when adding more eigenfunctions. We observe a reduction of the error as we use more and more additional coarse-grid basis functions. Also, we observe that the interior error is of comparable size (with either scaling) and that the interface error is bigger if we use the coarse penalty scaling.

We fix the number of additional eigenvectors L_i^{add} and compute the interior and boundary errors when the coarse solution is computed with different penalties. We note that the fine-scale solution is computed with the fine-grid scaling of the penalty bilinear form. We repeat this experiments with $L_i^{add} = 0, 1, \ldots, 10$. Results are shown in Fig. 5. From these results we observe that the boundary error for the coarse-grid solution is more sensitive to the variations in the scaling of the penalty. Indeed, for example $M = 10$, with $L_i^{add} = 4$, $i = 1, \ldots, N$, the optimal penalty coefficient is approximately 70. This set of experiments demonstrates that one needs to properly choose the penalty parameter in order to balance boundary and interior errors.

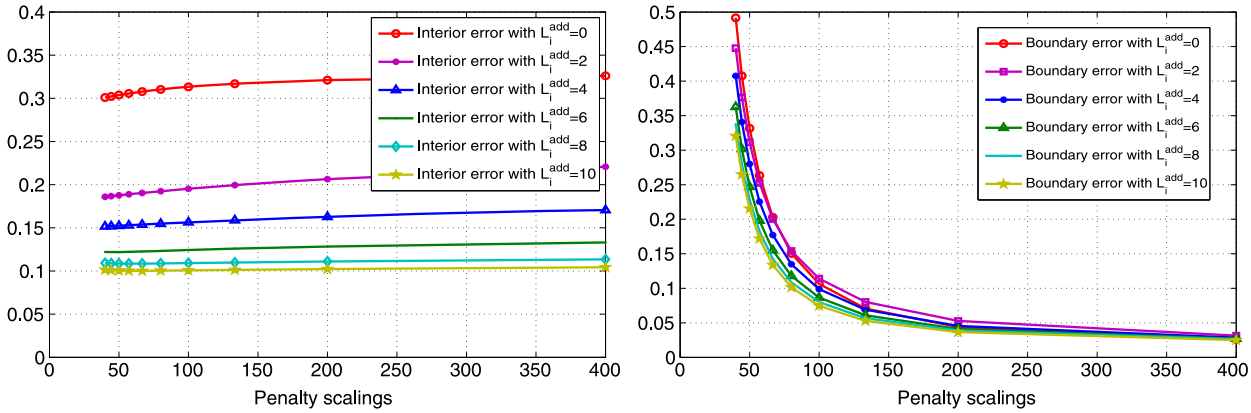

Fig. 5. The error for Method I (in Section 3.1) vs. penalty scaling for different values of L_i^{add}. Here $h = 1/100$, $H = 1/10$, and $\eta = 10^4$. The interior error (left) and the boundary error (right).

Table 2
Numerical results for Method I (Section 3.1) with increasing dimension of the coarse space, $h = 1/100$, $H = 1/10$, and $\eta = 10^4$. "Dim." stands for the dimension of the coarse space.

L_i^{add}	Dim.	Interface	Interior	Total	Energy	$\lambda_{\min}$
0	100	0.0318	0.2854	0.3172	0.3172	0.0528
2	300	0.0342	0.1679	0.2020	0.2646	0.0933
4	500	0.0257	0.1066	0.1323	0.1793	0.1165
6	700	0.0214	0.0800	0.1014	0.1444	0.2459
8	900	0.0194	0.0581	0.0775	0.1164	0.3514
10	1100	0.0185	0.0566	0.0751	0.1132	0.4551

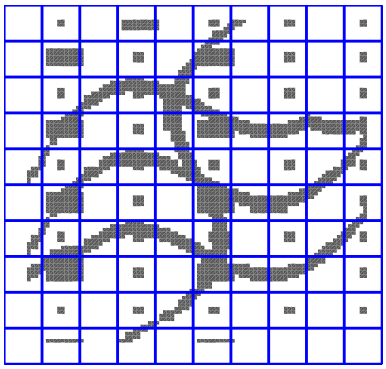

Fig. 6. High-contrast coefficient. Example 2.

4.3. Fine-grid snapshot space and amended eigenvalue problem

Next, we consider the method introduced in Section 3.1 with the amended eigenvalue problem. The convergence of this method, with respect to the number of eigenvectors used in the construction of the coarse space, follows from Theorem 3.6. We repeat the experiment described in Section 4.1 using the amended local eigenvalue problem. The results are displayed in Table 2 for the contrast $\eta = 10^4$. Similar results were observed for higher contrast ratios. We observe an error reduction when more eigenfunctions are added. Note that the results obtained by using the amended eigenvalue problem in Section 3.1 are slightly better compared when using the original eigenvalue problem. Our numerical results agree with our theoretical error estimates in Theorem 3.6. We also report the energy error.

Next, we consider another permeability field which is plotted in Fig. 6 with the contrast $\eta = 10^4$. This permeability field is more channelized compared with the permeability field in Fig. 1. We note that there are more asymptotically small eigenvalues in some subdomains as we observe in our numerical simulations. The numerical results are presented in Table 3 where we present interface, interior, total, and energy errors. We note that the convergence behavior is similar to the previous case with errors that are slightly smaller. These two high-contrast permeability examples show that our approach is capable of approximating the solution using local spectral multiscale basis functions.

Table 3
Numerical results for Method I (Section 3.1) with increasing dimension of the coarse space, $h = 1/100$, $H = 1/10$, and $\eta = 10^4$. The coefficient is depicted in Fig. 6. "Dim." stands for the dimension of the coarse space.

L_i^{add}	Dim.	Interface	Interior	Total	Energy	$\lambda_{\min}$
0	111	0.0643	0.2445	0.3088	0.4479	0.0237
2	311	0.0331	0.1072	0.1403	0.2048	0.0972
4	511	0.0228	0.0588	0.0817	0.1230	0.1946
6	711	0.0200	0.0437	0.0637	0.1014	0.2521
8	911	0.0189	0.0379	0.0567	0.0912	0.2838
10	1111	0.0187	0.0374	0.0560	0.0907	0.4613

Table 4
Numerical results for Method II (see Section 3.2) with increasing dimension of the coarse space, $h = 1/100$, $H = 1/10$, and $\eta = 10^4$. "Dim." stands for the dimension of the coarse space.

L_i^{add}	Dim.	Interface	Interior	Total	Energy	$\lambda_{\min}$
0	100	0.032	0.285	0.317	0.373	0.0528
2	300	0.034	0.168	0.202	0.265	0.0933
4	500	0.026	0.107	0.133	0.181	0.1165
6	700	0.021	0.079	0.101	0.144	0.2459
8	900	0.019	0.058	0.077	0.116	0.3514
10	1100	0.018	0.057	0.075	0.114	0.4552

Table 5
Numerical results for snapshot space and bilinear form m_i (instead of m_i^δ). Here $h = 1/100$, $H = 1/10$, and $\eta = 10^4$. "Dim." stands for the dimension of the coarse space.

L_i^{add}	Dim.	Interface	Interior	Total
2	300	0.0301	0.1750	0.2051
4	500	0.0278	0.1104	0.1382
6	700	0.0257	0.0905	0.1162
8	900	0.0243	0.0763	0.1007
10	1100	0.0223	0.0663	0.0986

4.4. Local solutions as snapshot space

Next, we consider the snapshot space given as in Section 3.2 that consists of a_i-harmonic functions defined in (26). We note that this snapshot space is used in the generalized multiscale finite element method for wave equation in [10]. The objective of presenting these results is to show that our proposed DG method is flexible and one can use various snapshot spaces.

In Table 4, we present the numerical results with contrast $\eta = 10^4$. Note, that we have obtained similar results for contrast $\eta = 10^6$ (not reported here). In this example, we choose $H = 1/10$ and the same setup as in the previous section. From these results we observe the convergence to the fine-grid solution of (3). We also observe that the error is inversely proportional to the λ_{min} (the minimum left out eigenvalue). Note that, we are reporting the error not with respect to the reference solution (on the snapshot space) but with respect to the fine-grid solution.

We recall that we need to use the bilinear form m_i^δ in the eigenvalue problem in order to obtain error estimates. We also observe convergence in the numerical tests if we use m_i bilinear form (instead of m_i^δ) in the snapshot space of harmonic functions. These results are reported in Table 5.

5. Discussions on the convergence

In this section, we discuss the convergence of the proposed discontinuous multiscale finite element method. For the multiscale method in Section 3.1, we derived error estimates in Theorem 3.6. Similar result holds for the coarse space described in Section 3.2. Despite of the fact we do not write an error estimate for the multiscale space using the original eigenvalue problem, which is a simple weighted eigenvalue problem, we verified its convergence in the numerical experiments. Moreover, we observe that the interface error due to penalty term is smaller than the interior error calculated with the energy norm (see Table 3). This indicates that once we have sufficient number of multiscale basis functions per coarse region (that are selected properly with our spectral problem) the interface error is dominated by the interior error. Consequently, one can argue that the local basis function construction should mostly take into account the approximation property within coarse regions the idea that we follow in this paper. The proposed eigenvalue problem attempts eliminating some interior degrees of freedom via (an interior and a boundary) mass matrix as discussed in our previous papers, e.g. [15,20]. By selecting mass matrix carefully in the local spectral problem, we represent piecewise constant functions within high-conductivity inclusions as the exact solution becomes almost constant within these regions. Note that without the κ

(or κ_{ij}) weight in the mass bilinear form, we will be selecting large number of important modes (all fine-grid degrees of freedom within high-conductivity regions according to previous studies).

We have amended the local spectral problem with a mass term on the boundary (see Sections 3.1 and 3.2) in order to obtain error estimates in terms of the local energy captured by the local space. A number of other similar eigenvalue problems that we tried, including adding some of the penalty terms in the eigenvalue problem, produced less satisfactory results.

We note that, even though the boundary error decreases, it is much lower than the interior error for relatively small penalty terms. Thus, if a small penalty term is preferred (e.g., for time-dependent problems), then one can attempt to find an optimal penalty. For the steady state problem considered in this paper, we do not investigate this problem. We believe that other appropriate techniques for coupling discontinuous spectral basis functions should be also considered. For instance, formulations that avoid the use of artificial penalty terms and use approaches such as hybridized discontinuous Galerkin methods, [11], or mortar methods, [6]. This is an object of the current research.

One can choose other multiscale spaces such that to achieve higher accuracy with lower degrees of freedom. For example, as we show that using the proper eigenvalue problem one can improve the error. The error to a reference solution can also be improved by selecting appropriate snapshot spaces. In general, the choice of snapshot space depends on the input space as discussed in the Introduction (see also [17] and the local solution space which this input space gives). Here, we do not explore the choice of snapshot spaces since our goal is to show that the discontinuous Galerkin method provides a nice framework to couple discontinuous basis functions computed locally.

6. Conclusions

In this paper, we propose generalized multiscale finite element methods for second order elliptic equations in the framework of the discontinuous Galerkin finite element method. We propose two different finite element spaces on the coarse mesh. The first space is based on a local eigenvalue problem that uses the sum of a weighted L_2-norm and a term related to the penalty for computing the "mass" matrix. For the construction of the second space, the local eigenvalue problem is solved in the snapshot space where the snapshots are chosen as harmonic extensions of unitary boundary functions. These multiscale basis functions are inherently discontinuous and SIPG coupling is used to couple these basis functions. We investigate the stability of the proposed methods and derive error estimates. Our results show that one needs to amend the mass matrix with a term related to the penalty. This allows obtaining error estimates and robust numerical results. In our numerical results, we compute the errors corresponding to the interior and the boundary. Our numerical results show that all methods perform similarly in the examples presented in the paper. We note that the second method or the use of snapshot spaces are recommended if one can estimate the error between the solution and its projection onto the snapshot space. By introducing an appropriate snapshot space, we can reduce the dimension of the local spectral problems. If one can not construct such space, one needs to use all the interior fine-grid degrees of freedom in solving an appropriate local spectral problems.

Acknowledgements

Y.E.'s work is partially supported by the US DoD, DOE and NSF (DMS 0934837, DMS 0724704, and DMS 0811180). J. Galvis would like to acknowledge partial support from DOE. R. Lazarov's research was supported in parts by NSF (DMS 1016525).

We are grateful to Mr. Chak Shing Lee for implementing one of the methods and providing the results reported in Table 5.

References

[1] J.E. Aarnes, On the use of a mixed multiscale finite element method for greater flexibility and increased speed or improved accuracy in reservoir simulation, Multiscale Model. Simul. 2 (2004) 421–439.
[2] J.E. Aarnes, Y. Efendiev, Mixed multiscale finite element for stochastic porous media flows, SIAM J. Sci. Comput. 30 (5) (2008) 2319–2339.
[3] T. Arbogast, Analysis of a two-scale, locally conservative subgrid upscaling for elliptic problems, SIAM J. Numer. Anal. 42 (2) (2004) 576–598 (electronic).
[4] T. Arbogast, K.J. Boyd, Subgrid upscaling and mixed multiscale finite elements, SIAM J. Numer. Anal. 44 (3) (2006) 1150–1171 (electronic).
[5] T. Arbogast, M.S.M. Gomez, A discretization and multigrid solver for a Darcy–Stokes system of three dimensional vuggy porous media, Comput. Geosci. 13 (2) (2009) 331–343.
[6] T. Arbogast, G. Pencheva, M.F. Wheeler, I. Yotov, A multiscale mortar mixed finite element method, Multiscale Model. Simul. 6 (1) (2007) 319–346.
[7] D.N. Arnold, F. Brezzi, B. Cockburn, L.D. Marini, Unified analysis of discontinuous Galerkin methods for elliptic problems, SIAM J. Numer. Anal. 39 (5) (2002) 1749–1779.
[8] S. Boyaval, C. LeBris, T. Lelièvre, Y. Maday, N. Nguyen, A. Patera, Reduced basis techniques for stochastic problems, Arch. Comput. Methods Eng. 17 (2010) 435–454.
[9] C.-C. Chu, I.G. Graham, T.-Y. Hou, A new multiscale finite element method for high-contrast elliptic interface problems, Math. Comput. 79 (272) (2010) 1915–1955.
[10] E.T. Chung, Y. Efendiev, W.T. Leung, Generalized multiscale finite element method for wave propagation, 2013, in preparation.
[11] B. Cockburn, J. Gopalakrishnan, R.D. Lazarov, Unified hybridization of discontinuous Galerkin, mixed, and continuous Galerkin methods for second order elliptic problems, SIAM J. Numer. Anal. 47 (2) (2009) 1319–1365.
[12] M. Dryja, On discontinuous Galerkin methods for elliptic problems with discontinuous coefficients, Comput. Methods Appl. Math. 3 (1) (2003) 76–85 (electronic). Dedicated to Raytcho Lazarov.

[13] W. E, B. Engquist, Heterogeneous multiscale methods, Commun. Math. Sci. 1 (1) (2003) 87–132.
[14] J. Eberhard, G. Wittum, A coarsening multigrid method for flow in heterogeneous porous media, in: Multiscale Methods in Science and Engineering, in: Lecture Notes in Computational Science and Engineering, vol. 44, Springer, Berlin, 2005, pp. 111–132.
[15] Y. Efendiev, J. Galvis, Coarse-grid multiscale model reduction techniques for flows in heterogeneous media and applications, in: Numerical Analysis of Multiscale Problems, in: Lecture Notes in Computational Science and Engineering, vol. 83, 2012, pp. 97–125.
[16] Y. Efendiev, J. Galvis, A domain decomposition preconditioner for multiscale high-contrast problems, in: Y. Huang, R. Kornhuber, O. Widlund, J. Xu (Eds.), Domain Decomposition Methods in Science and Engineering XIX, in: Lecture Notes in Computational Science and Engineering, vol. 78, Springer-Verlag, 2011, pp. 189–196.
[17] Y. Efendiev, J. Galvis, T. Hou, Generalized Multiscale Finite Element Methods (GMsFEM), J. Comput. Phys. 251 (2013) 116–135.
[18] Y. Efendiev, J. Galvis, R. Lazarov, J. Willems, Robust domain decomposition preconditioners for abstract symmetric positive definite bilinear forms, ESAIM Math. Model. Numer. Anal. 46 (5) (2012) 1175–1199.
[19] Y. Efendiev, J. Galvis, F. Thomines, A systematic coarse-scale model reduction technique for parameter-dependent flows in highly heterogeneous media and its applications, Multiscale Model. Simul. 10 (4) (2012) 1317–1343.
[20] Y. Efendiev, J. Galvis, X.H. Wu, Multiscale finite element methods for high-contrast problems using local spectral basis functions, J. Comput. Phys. 230 (2011) 937–955.
[21] Y. Efendiev, T. Hou, Multiscale Finite Element Methods: Theory and Applications, Surveys and Tutorials in the Applied Mathematical Sciences, vol. 4, Springer, New York, 2009.
[22] Y. Efendiev, T. Hou, V. Ginting, Multiscale finite element methods for nonlinear problems and their applications, Commun. Math. Sci. 2 (2004) 553–589.
[23] J. Galvis, Y. Efendiev, Domain decomposition preconditioners for multiscale flows in high contrast media, Multiscale Model. Simul. 8 (2010) 1461–1483.
[24] I.G. Graham, P.O. Lechner, R. Scheichl, Domain decomposition for multiscale PDEs, Numer. Math. 106 (4) (2007) 589–626.
[25] T. Hou, X.H. Wu, A multiscale finite element method for elliptic problems in composite materials and porous media, J. Comput. Phys. 134 (1997) 169–189.
[26] T. Hughes, G. Feijoo, L. Mazzei, J. Quincy, The variational multiscale method—a paradigm for computational mechanics, Comput. Methods Appl. Mech. Eng. 166 (1998) 3–24.
[27] O. Iliev, R. Lazarov, J. Willems, Variational multiscale finite element method for flows in highly porous media, Multiscale Model. Simul. 9 (4) (2011) 1350–1372.
[28] P. Jenny, S.H. Lee, H. Tchelepi, Multi-scale finite volume method for elliptic problems in subsurface flow simulation, J. Comput. Phys. 187 (2003) 47–67.
[29] S. Kaulmann, M. Ohlberger, B. Haasdonk, A new local reduced basis discontinuous Galerkin approach for heterogeneous multiscale problems, C. R. Acad. Sci. Paris, Ser. I 349 (23–24) (2011) 1233–1238.
[30] Y. Maday, Reduced-basis method for the rapid and reliable solution of partial differential equations, in: International Congress of Mathematicians, vol. III, Eur. Math. Soc., Zürich, 2006, pp. 1255–1270.
[31] A. Toselli, O. Widlund, Domain Decomposition Methods—Algorithms and Theory, Computational Mathematics, vol. 34, Springer-Verlag, 2005.
[32] P.S. Vassilevski, Multilevel Block-Factorization Preconditioners. Matrix-Based Analysis and Algorithms for Solving Finite Element Equations, Springer-Verlag, New York, 2008.
[33] P.S. Vassilevski, Coarse spaces by algebraic multigrid: multigrid convergence and upscaling error estimates, Adv. Adapt. Data Anal. 3 (1–2) (2011) 229–249.
[34] M.F. Wheeler, G. Xue, I. Yotov, A multiscale mortar multipoint flux mixed finite element method, ESAIM Math. Model. Numer. Anal. 46 (4) (2012) 759–796.